Appl Petrochem Res (2013) 3:117–129
DOI 10.1007/s13203-013-0042-x

KACST-FORUM

# Characterization and activity study of the Rh-substituted pyrochlores for $CO_2$ (dry) reforming of $CH_4$

**Devendra Pakhare · Hongyi Wu · Savinay Narendra · Victor Abdelsayed · Daniel Haynes · Dushyant Shekhawat · David Berry · James Spivey**

Received: 15 March 2013 / Accepted: 15 September 2013


**Abstract** Isomorphic substitution of Rh at varying levels on the B site of lanthanum zirconate pyrochlore ($La_2Zr_2O_7$; designated LZ) resulted in the formation of thermally stable catalysts suitable for fuel reforming reactions operating at 900 °C. Three specific catalysts are reported here: (a) unsubstituted lanthanum zirconate (LZ), (b) LZ with 2 wt% substituted Rh (L2RhZ), and (c) LZ with 5 wt% substituted Rh (L5RhZ). These catalysts were characterized by XRD, XPS, and $H_2$-TPR. XRD of the fresh, calcined catalysts showed the formation of the pyrochlore phase ($La_2Zr_2O_7$) in all three materials. In L5RhZ, the relatively high level of Rh substitution led to the formation of $LaRhO_3$ perovskite phase which was not observed in the L2RhZ and LZ pyrochlores. TPR results show that the L5RhZ consumed 1.57 mg $H_2/g_{cat}$, which is much greater than the 0.508 $H_2/g_{cat}$ and 0.155 mg $H_2/g_{cat}$ for L2RhZ and LZ, respectively, suggesting that the reducibility of the pyrochlore structure increases with increasing Rh-substitution. DRM was studied on these three catalysts at three different temperatures of 550, 575, and 600 °C. The results showed that $CH_4$ and $CO_2$ conversion was significantly greater for L5RhZ compared to L2RhZ and no activity was observed for LZ, suggesting that the surface Rh sites are required for the DRM reaction. Temperature programmed surface reaction showed that L5RhZ had light-off temperature 80 °C lower than L2RhZ. The spent catalysts after runs at each temperature were characterized by temperature programmed oxidation (TPO) followed by temperature programmed reduction and XRD. The TPO results showed that the amount of carbon formed over L5RhZ is almost half of that formed on L2RhZ.

**Keywords** Dry reforming · Lanthanum zirconate · Pyrochlores · Lattice oxygen · Isomorphic substitution · Perovskite · Reverse water gas shift

D. Pakhare · J. Spivey (✉)
Department of Chemical Engineering, Louisiana State University, Baton Rouge, LA 70803, USA
e-mail: jjspivey@lsu.edu

H. Wu
Department of Chemistry, Southern University, Baton Rouge, LA 70816, USA

S. Narendra
Department of Mechanical Engineering, Indian Institute of Technology, Kharagpur 721302, India

V. Abdelsayed · D. Haynes · D. Shekhawat · D. Berry
National Energy Technology Laboratory, U. S. Department of Energy, Morgantown, WV 26507, USA

## Introduction

Pyrochlores are a class of ternary metal oxides based on the fluorite structure with a cubic unit cell with a general formula of $A_2B_2O_7$. An important property of these materials is that catalytically active noble metals can be substituted isomorphically on the B site to form a crystalline catalyst. These materials consist of vacancies at the A and O sites, which facilitate oxygen ion migration within the structure [1]. The A site is usually a large cation (typically rare earth elements) and the B site cation has a smaller radius (usually transition metal) [2]. For the pyrochlore structure to be stable it is necessary that the ionic radius ratio of A and B site cations be between 1.46 and 1.78 [1]. The ratio of the ionic radii for $La_2Zr_2O_7$ is 1.61 [3]. If the ratio of the ionic radii is greater than 1.78, a perovskite phase can be formed. Below a ratio of 1.46 a fluorite structure is formed [4]. Catalytically active metals like Ru, Rh, Pt can be

substituted into the B site of the pyrochlore structure because they meet this ionic radius constraint and have the required oxidation state [5]. The resulting materials possess the thermal stability inherent in the pyrochlore structure, which also constrains the active metal within the pyrochlore structure even at high temperatures.

Steam reforming, autothermal reforming, and partial oxidation of methane are used to reform methane to synthesis gas [5–7]. $CO_2$ reforming of $CH_4$ is a highly endothermic reaction and has been widely studied on a number of catalysts [8–11]. For fuel reforming, one study shows that the activity decreases in the order Ru, Rh > Ir > Ni, Pt, Pd > Co > Fe, Cu [12], with noble metals also showing higher activity and greater resistance to deactivation by carbon deposition [13]. Carbide catalysts have also been used for studying this reaction [6, 14]. Economic evaluations have suggested a cost advantage for DRM as a route to the production of synthesis gas [15].

There are two major problems associated with dry reforming, (a) deactivation due to carbon formation on the catalyst, and (b) thermal degradation of the catalyst and/or support at the high temperatures required for this reaction, typically above 700 °C. Studies using non-noble metals like Fe, Ni, have consistently shown rapid deactivation by carbon deposition [16–18], although this can be minimized in some cases by maintaining high metal dispersion [17]. Because temperatures well above 700 °C are required to reach high syngas yields, traditional supported metals are not stable, suggesting the need to develop an inherently stable material that is catalytically active. Resistance to carbon formation is also related to the oxygen conductivity of substituted pyrochlores [19]. Oxygen mobility within the pyrochlore structure is a strong function of the La content in the structure. It is shown by Diaz-Guillen et al. [20] that the activation energy for oxygen ion conductivity decreases from 1.13 eV for $Gd_2Zr_2O_7$ to 0.81 eV for $GdLaZr_2O_7$ with an increase in the La substitution in the pyrochlore structure.

Although pyrochlores have the thermal stability and potential for active metals to be substituted into the structure, we are aware of only one report of DRM on any pyrochlore. Ashcroft et al. [21] studied pyrochlores based on Eu, Ru, Gd, but found that they decomposed into the various oxides at DRM conditions.

The present study focuses on the characterization and activity of Rh-substituted pyrochlores, which have been studied for reactions such as fuel reforming [19, 22]. Specifically, lanthanum zirconates (LZ) into which 2 and 5wt% Rh have been substituted at the B site of the pyrochlore structure are characterized by ICP, XRD, XPS, TPO and $H_2$-TPR. $La_2Zr_2O_7$ pyrochlores with Rh substitution on the Zr site (known as the B site, based on the general formula for pyrochlores as $A_2B_2O_7$) were tested for their activity at 550, 575 and 600 °C to study the kinetics of the reaction. Post-run temperature programmed oxidation (TPO) is used to determine the coke formation.

## Experimental section

### Catalyst synthesis

The LZ, L2RhZ and L5RhZ pyrochlores were synthesised by modified Pechini method [19]. The synthesis and ICP procedure had been reported earlier [5, 19].

### Catalyst characterization

The equipment and experimental procedure details for X-ray diffraction (XRD), X-ray photoelectron spectroscopy (XPS), $H_2$ temperature programmed reduction (TPR), temperature programmed surface reaction (TPSR) are reported in our earlier work [5]. For this work XPS spectra were obtained for the C 1 s, O 1 s, La 3d, Zr 3d, and Rh 3d. In each case, the binding energy (BE) and the area of the corresponding peaks were measured.

### Activity study

The composition of reactant gases used for the reaction over the catalyst was 10 mol% of $CO_2$/He and 10 mol% of $CH_4$/He. We studied the activity of the catalysts for DRM at different temperatures 550, 575, and 600 °C. The mass spectrometer (MS) connected to the reactor gave the mole fractions of the reactants in the blank condition. DRM was performed with an equimolar reactant feed of 20 mL/min of each of the reactant gases to give a total space velocity of 48,000 mL/$g_{cat}$/h. For each run, 50 mg of the catalyst was loaded in the U-tube reactor. Before each reaction run, the catalysts were heated to the reaction temperature in flowing He; no reduction was conducted before subjecting the catalysts to DRM. The reactants $CO_2$ and $CH_4$ were introduced after this into the reactor at desired flow rates. The mole fractions of the reactants and products from the mass spectrometer helped us to compare the results with the blank conditions.

### Temperature programmed oxidation (TPO)

After DRM, a TPO was conducted for studying the carbon formed during the reaction. For conducting the TPO, the catalyst was cooled to room temperature (ca. 35 °C) in flowing He at 20 mL/min. Then it was oxidized in flowing 5 % $O_2$/He at 30 mL/min from room temperature to 950 °C and the ramp rate was 5 °C/min. The conditions were maintained isothermal at 950 °C for 30 min. The CO

($m/z = 28$) and $CO_2$ ($m/z = 44$) emitted during the TPO were tracked using the mass spectrometer hooked up to the reactor outlet.

## Results and discussions

### X-ray diffraction study of fresh catalyst

Figure 1 shows the XRD patterns for the freshly calcined pyrochlores. The star marked peaks represent the $La_2Zr_2O_7$ (ICSD no: 50-0837) pyrochlore phase and the diffraction angle for these peaks is similar to the diffraction patterns observed in the literature [19, 23].

Haynes et al. [19] used L2RhZ pyrochlores for the partial oxidation of n-tetradecane, and their XRD pattern for pyrochlores match those in Fig. 1 for LZ and L2RhZ in this study. However, for L5RhZ there was an extra peak observed at ~32°. Gallego et al. [17] and Arauj et al. [11]. studied perovskites for DRM and observed main diffraction peak for $LaCoO_3$ and $LaRuO_3$, respectively, at ~32°. The similar peak observed at 32° in the XRD pattern for L5RhZ pyrochlore (Fig. 1) suggests that 5 wt% Rh substitution resulted in the formation of a separate $LaRhO_3$ perovskite phase.

To study effect of Rh substitution in further detail, XRD with a slow sweep rate was conducted on the fresh catalysts. Figure 2 shows the XRD pattern for a slow sweep rate; it is observed that there is a small peak for $LaRhO_3$ for the L2RhZ pyrochlore, but a prominent one for L5RhZ. The amount of Rh in the 5 % and the 2 % sample appears to be in excess of the maximum substitution limit of the pyrochlore structure, and thus resulted in the formation of a separate $LaRhO_3$ perovskite phase. Isomorphic substitution

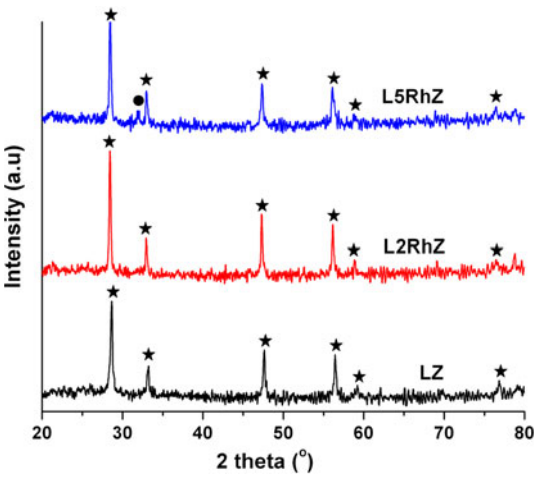


**Fig. 1** XRD pattern for freshly calcined LZ, L2RhZ, and L5RhZ pyrochlores (*star symbols* $La_2Zr_2O_7$, and *circles* $LaRhO_3$)

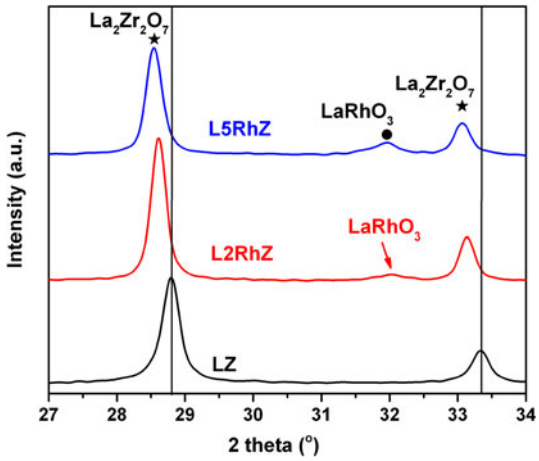


**Fig. 2** Slow scan XRD pattern for freshly calcined LZ, L2RhZ, and L5RhZ pyrochlores

of Rh on the B site has caused a small shift in the diffraction peak to a smaller angle for L2RhZ and L5RhZ compared to LZ. Lower diffraction angle corresponds to an increase in the lattice parameter of LRhZ catalysts due to Rh substitution.

### X-ray photoelectron spectroscopy of the fresh catalysts

XPS spectra for the Rh 3d core level obtained from L2RhZ and L5RhZ pyrochlores are shown in Fig. 3a, b, respectively.

In the deconvolution process, the relative intensity and separation of the spin–orbit for Rh $3d_{5/2}$–$3d_{3/2}$ doublet were fixed at ratio of 3:2 and 4.8 eV, respectively [24]. According to the literature, the BE of $Rh^0$ valence state is 307.1–307.6 eV and BE of $Rh^{3+}$ valence state is in a wide range from 308.8 to 311.3 eV depending on the surrounding environment [24–27]. For L2RhZ (see Fig. 3a), $Rh^{3+}$ was the only detected species as deduced from the binding energy of the Rh $3d_{5/2}$ photoelectron peak at 308.9 eV. Compared to L2RhZ, the valence state of Rh for L5RhZ is more complicated. For L5RhZ, the $Rh^{3+}$ is the dominant valance state with peak at 309.0 eV (see Fig. 3b); a smaller Rh $3d_{5/2}$ peak is observed at a lower binding energy of 308.3 eV which indicates the presence of another valence state of Rh. This peak at 308.3 eV is attributed to partially oxidized $Rh^{\delta+}$ species [25]. The relative distributions of $Rh^{3+}$ and $Rh^{\delta+}$ in L5RhZ are 82.8 and 17.2 %, respectively (see Table 1).

It should be noted that the FWHM (full width half maxima) of Rh peaks was significantly broader (2.0–2.7 in our measurement) when compared to those of Rh standard (about 0.7 for pure bulk $Rh_2O_3$). The broadening of Rh peaks may suggest a high dispersion of Rh in catalyst with little local aggregation [25, 28].

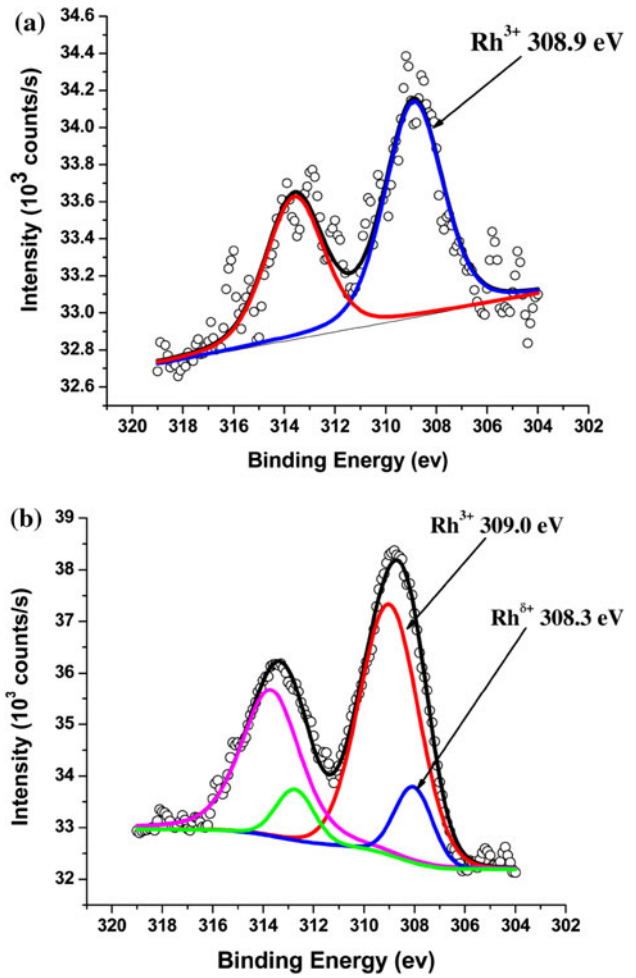


**Fig. 3** Photoelectron Rh 3d spectra for **a** L2RhZ, **b** L5RhZ pyrochlores

Quantitative analysis indicates the atomic percent of Rh on the surface of L2RhZ and L5RhZ pyrochlores is 0.78 and 3.15 %, respectively. This surface Rh concentration for individual pyrochlores is smaller than the theoretical levels obtained from inductively couple plasma-optical emission spectroscopy (ICP-OES) results (see Table 2). Since XPS is a surface sensitive technique which only can detect elements several nanometers under the surface, this result suggests that the remaining Rh lies within the lattice, as expected.

Both pyrochlores have surface Rh in similar oxidation states, but the absence of $Rh^{\delta+}$ signal for L2RhZ may be due to its lower Rh loadings, which limits the accuracy in deconvolution of the Rh peak due to high signal-to-noise level. The ratio of surface Rh concentration (by wt) for L5RhZ and L2RhZ is about (3.15:0.78 = 4), which is greater than their bulk ratio i.e., 4.4:1.7 = 2.6, as observed in the ICP-OES analysis. This indicates that the surface of L5RhZ is enriched with Rh compared to the surface of L2RhZ. As XPS detects elements within a few nanometers

**Table 1** XPS determined relative atomic ratio of surface Rh species in 2 and 5wt% Rh catalyst

| Catalyst | $Rh^{\delta+}/Rh_{total}$ (%) | $Rh^{3+}/Rh_{total}$ (%) |
|---|---|---|
| 2 wt% Rh | 0 | 100 |
| 5 wt% Rh | 17.2 | 82.8 |

**Table 2** Rh concentration (wt%) obtained by different methods

| Catalyst | Method for obtaining Rh concentration (wt%) | |
|---|---|---|
| | ICP-OES (bulk) | XPS (surface) |
| L2RhZ | 1.7 | 0.78 |
| L5RhZ | 4.4 | 3.15 |

depths from the surface, a higher surface concentration would mean that the surface Rh on L5RhZ is well dispersed. If there was any aggregation of Rh on the surface then the detected amount of Rh on L5RhZ surface would be less or close to that of L2RhZ. But a higher surface concentration indicates that the greater Rh loading in L5RhZ did not cause any local surface aggregation of Rh, which generally would decrease the detected surface concentration of the metal.

XPS analysis shows that for both L2RhZ and L5RhZ pyrochlores, the $3d_{5/2}$ peaks of La and Zr elements were 833.4–833.6 and 182.1–182.3 eV, respectively. These peaks positions indicated Zr and La in the pyrochlore structure and were in the $Zr^{4+}$ ($ZrO_2$) and $La^{3+}$ ($La_2O_3$) oxidation states, respectively [29, 30].

## Temperature programmed reduction (TPR)

Figure 4 shows the hydrogen TPR profiles for the three catalysts. The LZ pyrochlore reduction profile shows reduction peaks at 490 and 580 °C, corresponding to an $H_2$ consumption of 0.155 mg $H_2/g_{cat}$. This corresponds to 0.6 % reduction of the lanthanum zirconate. The TPR profile of L2RhZ shows three distinct peaks at 380, 455, and 570 °C. All three catalysts show two peaks above 450 °C, which can be attributed to reduction of the LZ itself.

Comparison of the L2RhZ and LZ TPR results suggests that the 380 °C peak is due to reduction of Rh that is interacting strongly with the pyrochlore. The small additional peak 280 °C for L2RhZ may be due to reduction of Rh that is less strongly interacting with the pyrochlore [19]. For L5RhZ the 410 °C peak is close to that at 380 °C for the L2RhZ, and its larger area is consistent with the larger amount of reducible Rh in this catalyst. The similarity of the peak temperatures for this peak and that of the L2RhZ (410 versus 380 °C) indicates that the strength of the

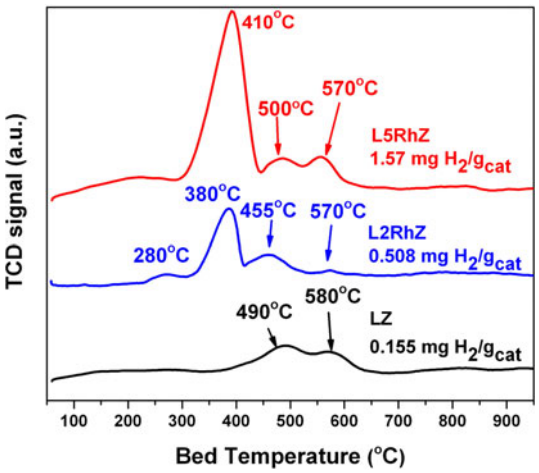


**Fig. 4** Temperature programmed reduction of freshly calcined LZ, L2RhZ, L5RhZ pyrochlores

interaction of this reducible Rh is similar on both catalysts. The L2RhZ consumed 0.508 mg $H_2/g_{cat}$, which includes $H_2$ consumed for the reduction of the Rh species at 380 °C and a small portion of the lanthanum zirconate at 455 °C and 570 °C. The $H_2$ consumption for L5RhZ is 1.57 mg $H_2/g_{cat}$. It is difficult to quantify exactly the percentage of reduction of Rh in the pyrochlore structure due to overlapping reduction peaks of Rh and lanthanum zirconates. However, the $H_2$ consumption by L2RhZ and L5RhZ is smaller than their respective theoretical consumption assuming complete Rh reduction (and no reduction of the pyrochlore) i.e., 0.66 mg $H_2/g_{cat}$ for L2RhZ and 1.7 mg $H_2/g_{cat}$ for L5RhZ. This means that a significant portion of the Rh is substituted in the bulk of the pyrochlore and is not available during the reduction reaction, as expected.

TPR profiles obtained in this study are similar to the ones observed by Haynes et al. [19]. The peak observed for LZ in our study shows two types of reducing species, one at 490 °C and the other at 580 °C. Whereas, the one observed by Haynes et al. [19], for LZ has a single peak at 527 °C. This difference in the reduction peaks could be due to the difference in the hydrogen concentration in the two TPR procedures. The concentration of the gas used for TPR in the work by Haynes et al. [19] was 5 % $H_2$/Ar and the one used in this work was higher 10 % $H_2$/Ar keeping the same ramp rate and flow rate. The higher partial pressure of the reducing gas in the present work resulted in a faster reduction reaction, allowing a distinction to be made between reduction peaks that were not visible in the Haynes et al. [19] study. The single broad peak observed by Haynes et al., thus appeared as a double peak in the present work.

The deconvoluted TPR profiles of LZ, L2RhZ, and L5RhZ pyrochlroes are shown in Fig. 5a–c, respectively (these figures differ in *y*-axis scale). Figure 5a shows that the LZ reduction peaks involve the reduction of four species. XPS results show that La and Zr are present in +3 and +4 oxidation states, respectively, in the pyrochlore structure. Peaks at 490 and 580 °C could be due to the reduction of $La^{+3}$ and $Zr^{+4}$ species [31]. The lower temperature peaks at 396 and 430 °C (not visible in Fig. 4 due to the *y*-axis scale) could be due to the reduction of partially coordinated lanthanum or zirconium cations at the surface. Hoang et al. [31] conducted TPR of the $ZrO_2$ support and lanthana promoted zirconia structure ($La_2O_3$–$ZrO_2$). They observed a reduction peak at 574 °C for $ZrO_2$ and at 554 °C for $La_2O_3$–$ZrO_2$ [31]. The high temperature peaks at 490 and 580 °C can be attributed to the reduction of $La_2O_3$–$ZrO_2$ and $ZrO_2$ phase, respectively [31]. In Fig. 5b, L2RhZ has a small peak at 280 °C appears to be due to the reduction of a weakly interacting Rh species [19]. The intensity of this peak is very low and thus this reducing species could not be accurately determined and deconvoluted during the analysis of the XPS peaks. Peaks at 375 and 394 °C can be assigned to the reduction of Rh with varying degrees of interaction with oxygen and neighboring atoms in the bulk of the pyrochlores. The 394 °C peak could also be due to the reduction of some lanthanum zirconate species reducing at 396 °C as seen in Fig. 5a. As mentioned earlier, the lanthanum zirconate is reduced at 430 and 490 °C (see Fig. 5a). The peak at 455 °C (in Fig. 5b) could be due to the reduction of these lanthanum zirconate species which have different levels of interaction with the neighboring metals due to Rh substitution in the pyrochlore structure compared to the unsubstituted LZ pyrochlore.

Deconvoluted TPR peaks for L5RhZ (Fig. 5c) show that there are peaks at 352, 396, and 416 °C. The 352 °C peak is likely to be due to the reduction of $Rh^{\delta+}$ species as observed in XPS results. The 396 and 416 °C peaks can be assigned to the reduction of bulk Rh with varying interaction with the pyrochlore structure. These species reducing at 396 and 416 °C have similar oxidation states and thus could not be distinctly determined during XPS analysis. Some portion of the 396 °C peak could be due to the reduction of the lanthanum zirconates as seen in Fig. 5a. The high temperature peaks at 500 and 570 °C are primarily due to the reduction of the same lanthanum and zirconium species as seen in Fig. 5a.

There are some apparent differences in the oxidized species observed in the TPR results and the XPS results. This is because the fresh catalysts, after calcination at 1,000 °C for 8 h as the final step in the synthesis process, were pretreated prior to the TPR in flowing oxygen up to 950 °C, whereas the catalysts used for XPS were not pretreated, although they were also calcined at 1,000 °C for 8 h. It is clear from the above deconvoluted TPR peaks that no peak can be assigned solely to the reduction of a particular metal

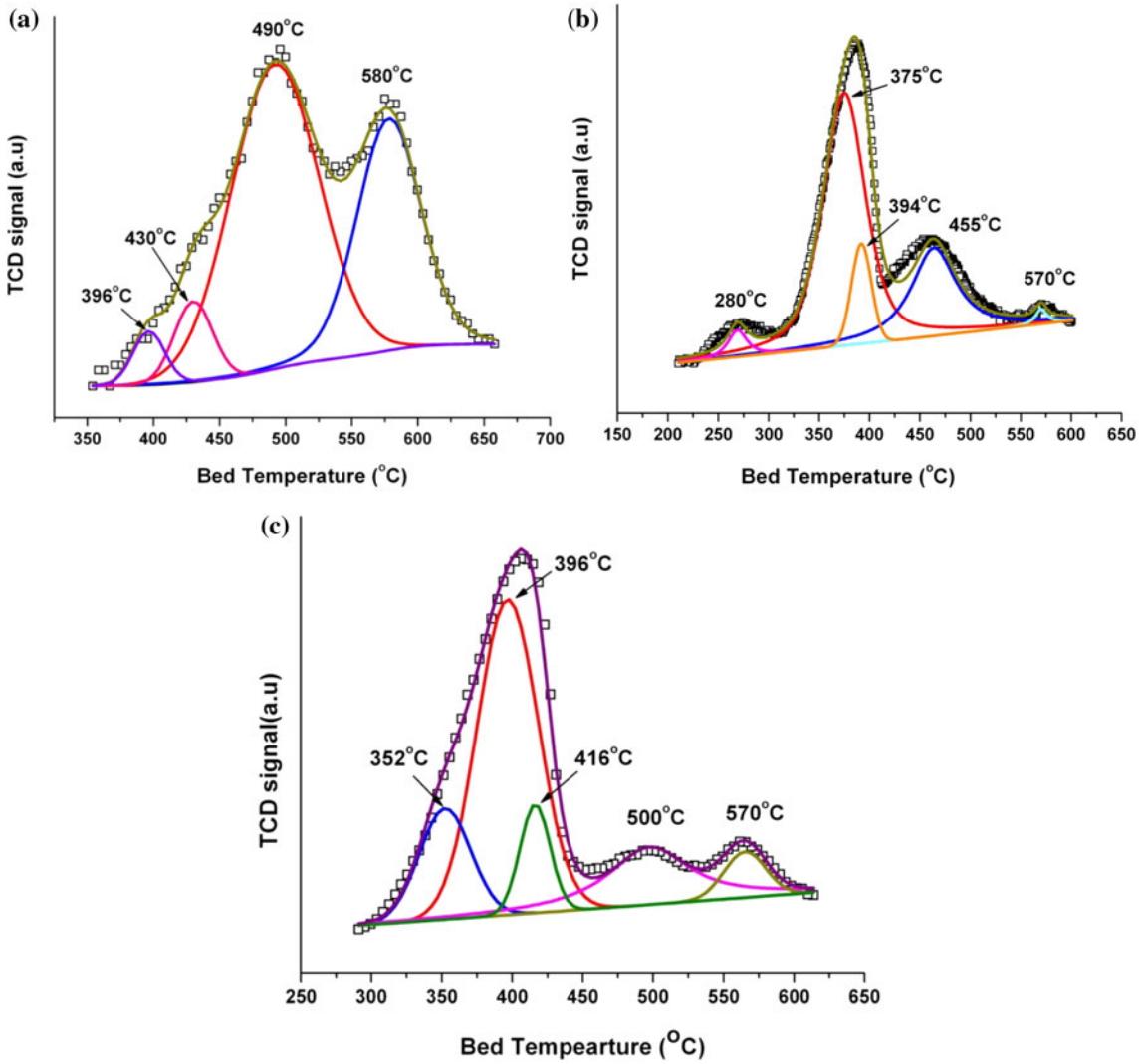


**Fig. 5** Deconvoluted TPR profiles of freshly calcined **a** LZ, **b** L2RhZ, and **c** L5RhZ

species. Lanthanum zirconate reduction peaks overlap with the reduction peaks for Rh in the pyrochlore. Thus, quantification of the percentage of Rh reduction in these pyrochlores cannot be performed using TPR.

## Temperature programmed surface reaction (TPSR)

TPSR was performed on LZ, L2RhZ, and L5RhZ and the product composition is plotted in Fig. 6a–c, respectively, as a function of temperature. For L2RhZ (Fig. 6b), there is no CO or $H_2$ formation observed until ~490 °C, but over L5RhZ (Fig. 6c) product formation begins at ~410 °C. Small but measurable water formation is observed over both the catalysts after light-off, which suggests that the RWGS takes place over both the catalysts up to ~700 °C. Assuming the rate determining step is the breaking of the C–H bond in $CH_4$ to form $CH_x$ surface species [32], and that this step occurs over Rh sites [33], the L5RhZ, which has more surface Rh sites (shown by XPS and TPR), enhances $CH_4$ activation and accelerates the reforming reaction rate compared to L2RhZ. This faster reaction rate over L5RhZ results in a lower light-off temperature i.e., 410 °C, compared to 490 °C for L2RhZ.

## Temperature effects on activity

### *Effect on $CH_4$ conversion ($X_{CH_4}$)*

Figure 7 shows the conversion of $CH_4$ ($X_{CH_4}$) for all three catalysts at each temperature as a function of time. The values on the right hand *y*-axis show the thermodynamic equilibrium values at that particular temperature. $X_{CH_4}$ over LZ pyrochlores was between 0.5 and 0.8 %, and was constant at all temperatures. This lower conversion is due to absence of any catalytically active Rh site on the surface of the LZ pyrochlore.

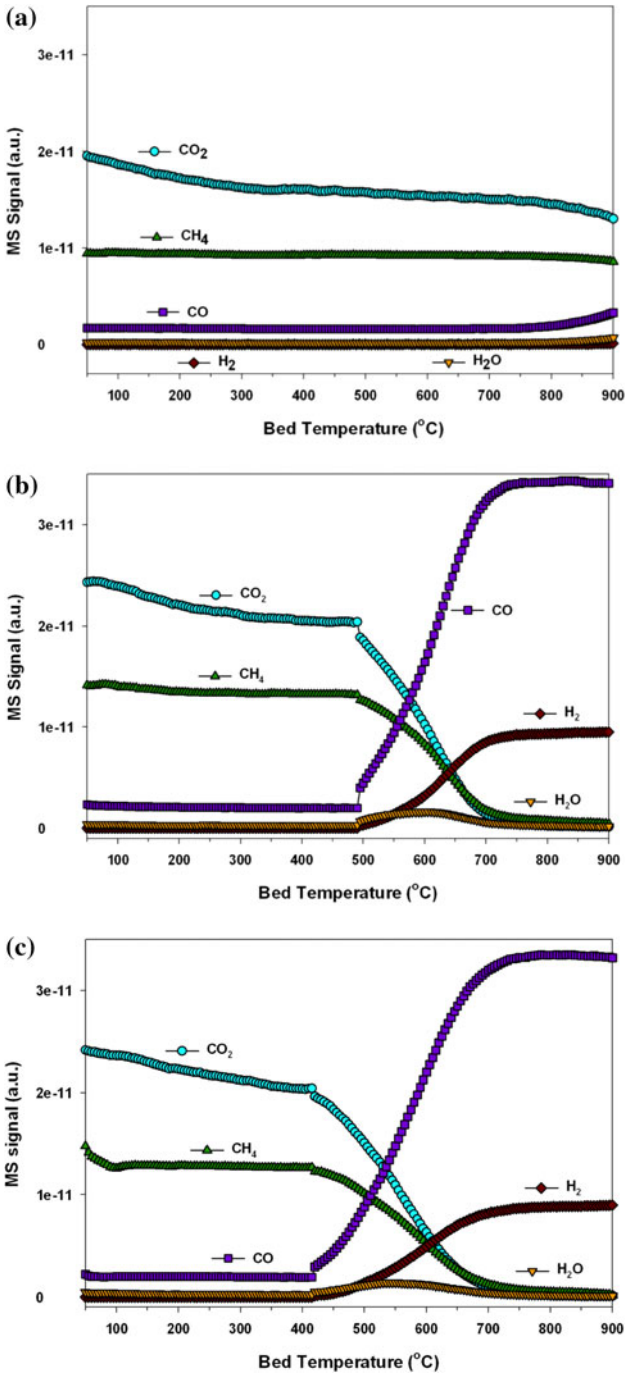


**Fig. 6** TPSR plots for **a** LZ, **b** L2RhZ, and **c** L5RhZ at in the temperature range 50–900 °C at 1 atm and GHSV = 48,000 mL/$g_{cat}$/h

The catalysts do not reach equilibrium at these temperatures. For the two Rh-containing catalysts, $X_{CH_4}$ increases with time. This increase could be attributed to the in situ reduction of the catalyst by $CH_4$. The catalysts used in this study were not reduced as a part of pre-treatment before conducting the reaction. As a result, the catalysts are likely initially reduced in situ by $CH_4$ then reduced by CO and $H_2$ as they are formed [21]. However, this in situ reduction by CO and $H_2$ could be slower than that in $H_2$-TPR due to lower concentration of $H_2$ during reaction. Ashcroft et al. [21] proposed this in situ reduction in their study of DRM over $Eu_2Ir_2O_7$ pyrochlores[21]. In-situ reduction of the catalyst would increase the number of available active metal sites with time thus increasing the conversion of $CH_4$ with time-on-stream.

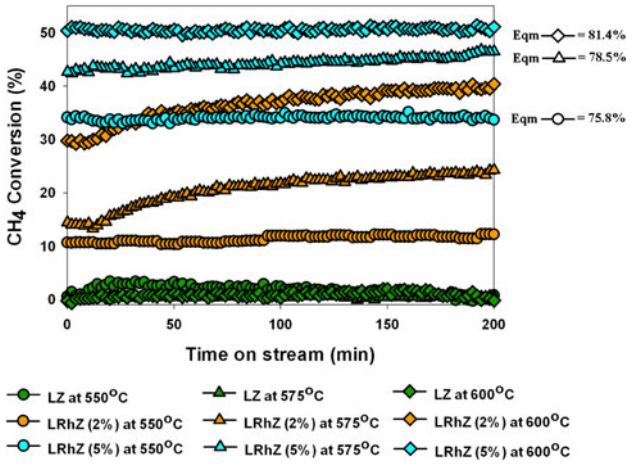


**Fig. 7** $CH_4$ conversion for LZ, L2RhZ and L5RhZ pyrochlores at 550, 575, and 600 °C at 1 atm and GHSV = 48,000 mL/$g_{cat}$/h. The values on the *right* hand *y*-axis show the thermodynamic equilibrium values at that particular temperature as obtained from equilibrium calculations

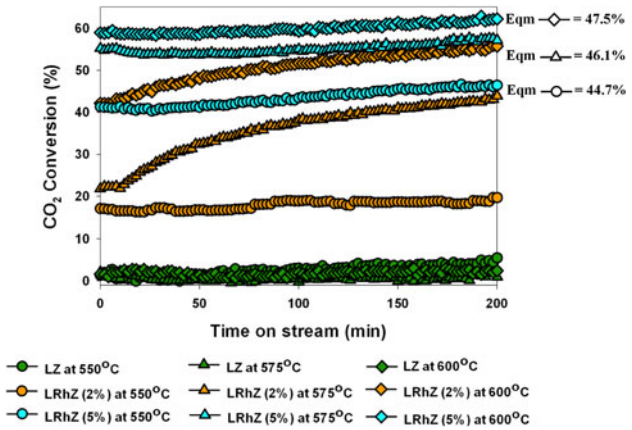


**Fig. 8** $CO_2$ conversion for LZ, L2RhZ and L5RhZ pyrochlores at 550, 575, and 600 °C at 1 atm and GHSV = 48,000 mL/$g_{cat}$/h. The values on the *right* hand *y*-axis show the thermodynamic equilibrium values at that particular temperature as obtained from equilibrium calculations

Iglesia and co-workers [32, 34], demonstrated that the rate of methane consumption on $Rh/Al_2O_3$ is first order in $CH_4$ concentration, and is independent of $CO_2$ concentration i.e., $r_{CH4} = kP_{CH4}$. They also demonstrated that the active site for DRM is Rh site and the lack of any significant activity for the LZ catalyst shows that Rh sites are

required to catalyze this reaction. The TPR and XPS results show that L5RhZ has more active Rh on the surface compared to L2RhZ and LZ. Thus, it would be expected that L5RhZ will have higher $X_{CH_4}$ than L2RhZ and LZ, as shown in Fig. 7. This is consistent with the results of Verykios et al. [35], who showed that during DRM, breaking of $CH_4$ to $CH_x$ ($x = 1$–3) on the Rh sites is the slow step in the reaction mechanism and determines the overall kinetics of the reaction over $Rh/Al_2O_3$. Thus, higher metal loading would kinetically favor the activation of methane and DRM.

*Effect on $CO_2$ conversion ($X_{CO_2}$)*

The conversion of $CO_2$ ($X_{CO_2}$) as a function of time for these catalysts is shown in Fig. 8. The average $X_{CO_2}$ for LZ was insignificant and independent of temperature. $X_{CO_2}$ for L5RhZ is substantially greater than that for L2RhZ at all temperatures.

For L2RhZ, the experimental $X_{CO_2}$ value at 550 °C is constant with time at ~18 %, which is substantially lower than the equilibrium value of 44.7 % (see Fig. 8). When the temperature is further increased to 575 and 600 °C, the experimental $X_{CO_2}$ for L2RhZ increases with time, and reaches a value close to equilibrium at 575 °C and greater than equilibrium value of 47.5 % at 600 °C after 200 min on stream. For L5RhZ, the experimental $X_{CO_2}$ increases slightly with time at all temperatures, and is consistently greater than the equilibrium values at all temperatures except 550 °C, where it is ~41 % versus equilibrium of 44.7 %. Equilibrium values of $X_{CH_4}$ and $X_{CO_2}$ were computed by considering $C_{(s)}$ as one product. Thermodynamically, $C_{(s)}$ formation is significant at these temperatures and the conversion of $CO_2$ is limited. It appears that carbon formation is kinetically limited on these catalysts, (as will be seen in the later $H_2/CO$ ratio results) compared to DRM and the reverse water gas shift (RWGS), allowing $X_{CO_2}$ to be greater than the thermodynamic equilibrium values calculated when $C_{(s)}$ is included in the calculation.

Previous studies show that $CO_2$ is activated by the support to form carbonate species and not by the active metal during DRM over conventional supported catalysts such as $Rh/Al_2O_3$ and $Rh/La_2O_3$ [33, 35–37]. Verykios and co-workers [35] while comparing $Ni/La_2O_3$ and $Ni/Al_2O_3$ catalysts for DRM showed that in the presence of $La_2O_3$; activation of $CO_2$ occurs via formation of $La_2O_2CO_3$. They proposed that the basic nature of $La_2O_3$ assists in the activation of $CO_2$ in the presence of surface $CH_x$ species on the metal or the metal support interface. It can be postulated that, in our case, the lanthanum zirconate assists in the activation of $CO_2$ to form adsorbed carbonate species. The adsorbed carbonate species are then reduced to form

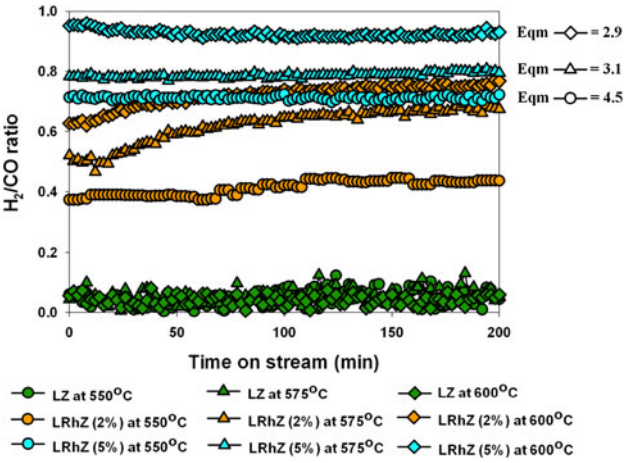


**Fig. 9** $H_2/CO$ ratio for LZ, L2RhZ and L5RhZ pyrochlores at 550, 575, and 600 °C at 1 atm and GHSV = 48,000 mL/$g_{cat}$/h. The values on the *right* hand *y*-axis show the thermodynamic equilibrium values at that particular temperature as obtained from equilibrium calculations

CO by the adsorbed $CH_x$ species formed on the Rh sites [35, 36, 38]. In case of LZ pyrochlore, there is no activation of $CH_4$ molecule since there are no Rh sites, thus reduction of $CO_2$ is limited at all temperatures, consistent with the results in Fig. 8.

If $CH_x$ species enhance the reduction of $CO_2$ to CO, it would be expected that $X_{CO_2}$ for L5RhZ will be greater than L2RhZ. The experimental results are in agreement with this hypothesis; $X_{CO_2}$ is greater for L5RhZ than for L2RhZ (Fig. 8).

*Effect on $H_2/CO$ ratio*

The $H_2/CO$ ratio plots for the three catalysts at 550, 575, and 600 °C are shown in Fig. 9. The $H_2/CO$ ratio for LZ pyrochlore was found to be close to 0.05 at all bed temperatures which is negligible and was constant throughout the time on stream. The $H_2/CO$ ratio for L5RhZ was considerably greater than for L2RhZ at all reaction temperatures (see Fig. 9).

The product stream consisted mainly of $H_2$ and CO, with a consistently lower $H_2/CO$ ratio than equilibrium at all temperatures. As mentioned earlier, thermodynamic calculations show that equilibrium amounts of $C_{(s)}$ are significant at these conditions. High levels of carbon formation would limit the formation of CO and thus increases equilibrium $H_2/CO$ ratios. However, it can be postulated that the rate of carbon formation on these catalysts is kinetically limited, favoring DRM and RWGS. DRM results in the $H_2/CO$ ratio of unity but due to the simultaneous occurrence of RWGS, the $H_2/CO$ ratio drops below equilibrium. Thus, comparing the $H_2/CO$ ratio for L2RhZ and L5RhZ; the $H_2/CO$ ratio of L5RhZ is

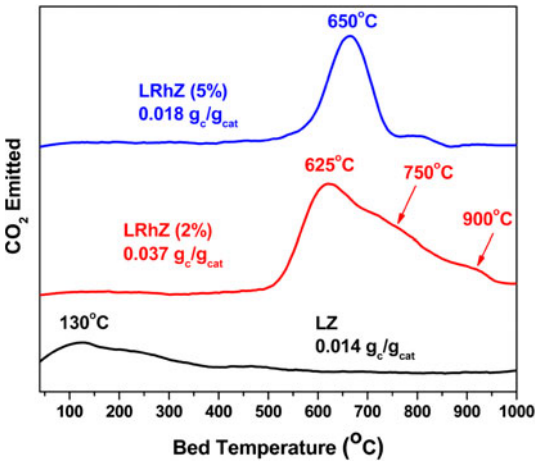


**Fig. 10** TPO profile for the catalysts spent at 550 °C, GHSV = 48,000 mL/$g_{cat}$/h at 1 atm

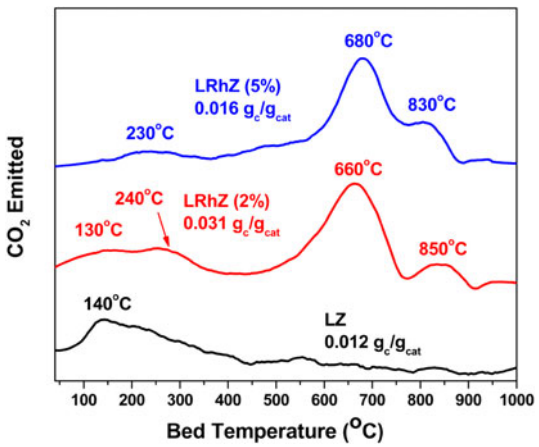


**Fig. 11** TPO profile for the catalysts spent at 575 °C, GHSV = 48,000 mL/$g_{cat}$/h at 1 atm

consistently greater and closer to unity than L2RhZ. This suggests greater rate of DRM than RWGS over L5RhZ compared to L2RhZ. Thus, increasing Rh substitution helps in limiting simultaneous reactions like RWGS and favors DRM.

The $H_2$/CO ratio for L2RhZ increases with time, particularly at 575 and 600 °C suggesting increase in the rate of DRM compared to RWGS. A similar increasing trend was also observed for the conversion of $CH_4$ (see Fig. 7), suggesting that the rate of DRM reaction increases with that of the activation of $CH_4$.

## Characterization of the spent catalyst

### *TPO (carbon burn-off) of the spent catalysts*

Immediately after performing DRM over these three catalysts, the spent catalysts were subjected to in situ TPO. The

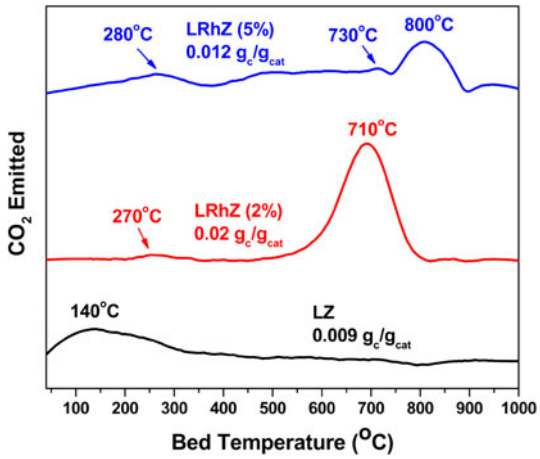


**Fig. 12** TPO profile for the catalysts spent at 600 °C, GHSV = 48,000 mL/$g_{cat}$/h at 1 atm

**Table 3** Summary of the carbon formed over the catalysts during the time on stream

| Bed temperature (°C) | Carbon formed ($g_{carbon}/g_{catalyst}$) | | |
|---|---|---|---|
| | LZ | L2RhZ | L5RhZ |
| 550 | 0.014 | 0.037 | 0.018 |
| 575 | 0.012 | 0.031 | 0.016 |
| 600 | 0.009 | 0.02 | 0.012 |

$CO_2$ signal during TPO of spent catalysts tested at 550, 575, and 600 °C is plotted in Figs. 10, 11, and 12, respectively. The amount of carbon formed during the reaction was quantified and is summarized in Table 3. The total amount of carbon formed over L5RhZ is roughly half of the amount of carbon formed over L2RhZ in each experiment.

A general mechanism can be postulated based on activation of $CH_4$ molecule on metallic sites to produce adsorbed $CH_x$ species ($x = 1$–3) [33]. These $CH_x$ species can be further reduced to surface carbon on the metal sites, which can react with $CO_2$ (DRM), or form surface carbon, leading to deactivation [36]. The TPO results (Figs. 10, 11, 12) show that although there was carbon deposited on all three catalysts, there was no observable decrease in activity with time on stream, up to 200 min, likely due to the slow axial growth of the deactivated portion of the catalyst bed.

*Catalyst spent at 550 °C* TPO profile for the catalyst spent at 550 °C (Fig. 10) shows that for LZ, a single broad peak was observed at 130 °C. This peak at ~100–130 °C is presumably due to the oxidation of the carbon with a relatively high H/C ratio [39]. For L2RhZ, single broad peak was observed at 625 °C. This broad peak overlaps other small peaks at higher temperatures of 750 and

900 °C. This suggests that there are at least two more forms of carbon formed over L2RhZ during the reaction. The peak at 625 °C is attributed to the oxidation of dehydrogenated form of carbon deposited on or near the metal site [22]. The higher temperatures that are overlapped by the 625 °C peak could be due to the oxidation of less reactive carbon species or the graphitic form of carbon which could be present away from the Rh site [22, 40]. TPO profile for L5RhZ shows a single identifiable peak at 650 °C attributed to dehydrogenated form of carbon which is very similar to the 625 °C peak observed over L2RhZ. A shoulder was observed for L5RhZ at 830 °C. This shoulder is most likely due to the oxidation of the less reactive graphitic carbon which is similar to that observed for L2RhZ at higher temperatures. Peaks at 750 and 900 °C (for L2RhZ) are not observed for L5RhZ; this could be due to the greater surface coverage of Rh on L5RhZ compared to L2RZ.

*Catalyst spent at 575 °C* Figure 11 shows the TPO profile for the catalyst spent at 575 °C for the three catalysts. The unsubstituted LZ pyrochlore shows a single broad oxidation peak at 140 °C. This peak is most likely due to the oxidation of reactive hydrogenated polymeric carbon with greater H/C ratio compared to the high temperature carbon. This peak at 140 °C is similar to the one observed over LZ spent at 550 °C (see Fig. 10). There were four types of oxidation peaks observed for L2RhZ, indicating formation of a corresponding number of different species of surface carbon. The peak at 130 °C could be due to the reactive form of carbon with a high H/C ratio as seen on the LZ pyrochlore. The 240 °C peak could be attributed to carbon with H/C ratio lower than that corresponding to the peak at 140 °C. It could also be the same carbon as 140 °C but situated away from the surface metal [39]. Thus, the peak at 660 °C may be attributed to hydrogenated carbon deposited on the metal atom while the 850 °C peak could be due to the oxidation of highly unsaturated carbon deposited over the non-active sites (i.e., lanthanum zirconate in our case) or further away from the Rh site. Peaks observed for L5RhZ are at 230, 680 and 830 °C which are similar to the ones observed for L2RhZ. The species of the carbon oxidized at these temperatures would be qualitatively the same as those oxidized over L2RhZ.

*Catalyst spent at 600 °C* TPO profile for LZ pyrochlores spent at 600 °C (shown in Fig. 12) shows a peak at 140 °C which is similar to the peaks observed over LZ spent at 550 °C (see Fig. 10) and 575 °C (see Fig. 11). L2RhZ TPO profile shows a very small peak at 270 °C followed by a large peak at 710 °C. The peak at 270 °C is due to the oxidation of hydrogenated carbon which is qualitatively similar to the 240 °C peak for L2RhZ in Fig. 11. The peak at 710 °C could be due to the dehydrogenation of the carbon formed further away from the active metal site which is oxidized at high temperatures. The graphitic nature of the carbon oxidized at 710 °C could be similar to the one observed in the superimposed peaks at 750, and 900 °C in Fig. 10 for L2RhZ. The TPO profile for L5RhZ has a small hump at 280 °C which is similar to the 270 °C peak for L2RhZ in the same plot. There is a very small peak observed at 730 °C which could be assigned to the same species as seen over the L2RhZ at 710 °C. A peak at 800 °C is observed for L5RhZ which was not seen over L2RhZ, this could be due to the deposition of dehydrogenated or graphitized carbon which is not in the proximity of the metallic site [40].

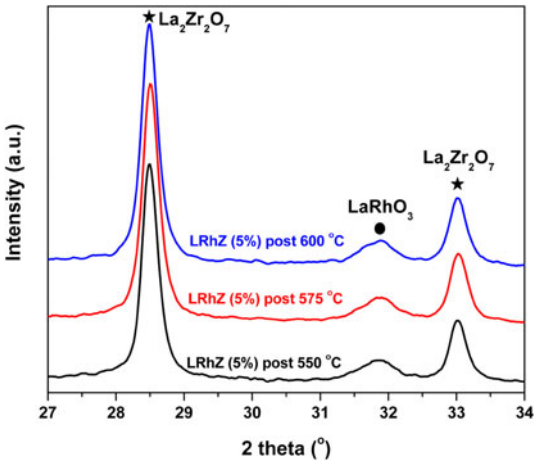


**Fig. 13** Plot of the XRD pattern for the L5RhZ pyrochlores spent for DRM at 500, 575, and 600 °C with GHSV = 48,000 mL/$g_{cat}$/h at 1 atm followed by TPO showing in particular the formation of the $LaRhO_3$ perovskite phase

*XRD of the spent catalyst from DRM and TPO*

The diffraction pattern of the spent LZ and L2RhZ pyrochlores resembled the pattern for the fresh catalyst (thus not shown here). There was no apparent shift in the peaks for $La_2Zr_2O_7$ or formation of any perovskite phase observed for LZ and L2RhZ. This shows that LZ and L2RhZ pyrochlores maintained their structure ($La_2Zr_2O_7$) after catalyzing the reaction under reducing reforming condition at these temperatures.

However, for L5RhZ spent catalysts, there was a peak observed at about 32° which could be assigned to the formation of a separate perovskite ($LaRhO_3$) phase. The magnified image of the XRD pattern for 27°–34° is shown in Fig. 13; this plot shows clearly the formation of the perovskite peak at these reaction temperatures. This peak ($LaRhO_3$) was also observed in the fresh L5RhZ catalysts but it was not as prominent compared to the other $La_2Zr_2O_7$ peaks. After subjecting the catalysts to the reducing

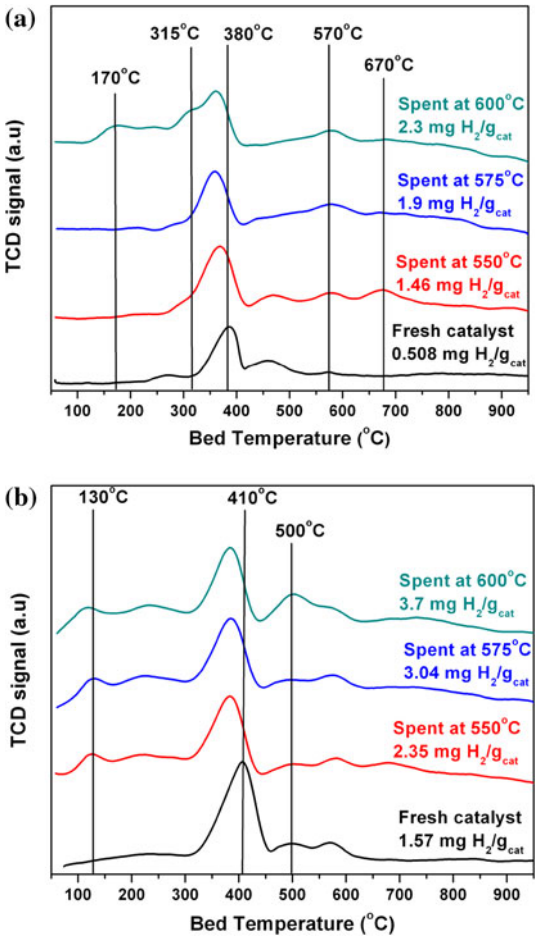


**Fig. 14** Temperature programmed reduction by $H_2$ of the catalysts spent for DRM at different temperatures and TPO **a** L2RhZ, and **b** L5RhZ. Reduction conducted from 50 to 950 °C ramping at 5 °C/min

reaction conditions followed by oxidation, this particular peak for $LaRhO_3$ at 32° becomes apparent.

*TPR by $H_2$ of the spent catalysts from DRM and TPO*

To study the changes in the reducibility of LZ and of Rh in the L2RhZ and L5RhZ pyrochlores, TPR was conducted on each spent catalyst after (a) DRM at different temperatures and (b) TPO. The TPR plots obtained from these spent catalysts are compared to the plots of the freshly calcined catalysts and the plots for L2RhZ and L5RhZ in Fig. 14a, b, respectively.

A qualitative and quantitative change was observed in the reduction profiles of L2RhZ pyrochlore (see Fig. 14a). The fresh catalyst had a reduction peak at 380 °C which is shifted consistently to a lower temperature in the reduction profiles of the spent catalysts, suggesting a slight increase in the reducibility Rh in the pyrochlore structure. When the reaction temperature was 600 °C; there was a low temperature peak observed at 170 °C and a shoulder at 315 °C, which was not seen in the other L2RhZ profiles. These peaks could be attributed to Rh that is less strongly bound to the pyrochlore structure which developed after DRM/TPO conditions. The quantitative increase in the $H_2$ consumption after DRM/TPO could be attributed partly to the reduction of the lanthanum zirconate at 570 °C and reduction of Rh at lower temperatures.

A comparison of the reduction profiles for fresh L5RhZ and those spent after DRM/TPO is shown in Fig. 14b. For the spent L5RhZ pyrochlores; a low temperature reduction peak was observed at 130 °C which was absent in the profile of fresh L5RhZ. In the TPR study by Haynes et al. [19] a reduction peak at 136 °C for $Rh/Al_2O_3$ was attributed to the reduction of supported Rh with weaker interaction with the support. This suggests that Rh that was substituted in the pyrochlore structure during calcination; apparently comes out of the structure to the surface of the pyrochlore as a result of the DRM/TPO reactions. This surface Rh is similar to the Rh observed on the supported $Rh/Al_2O_3$ catalysts in terms of the reducibility [41]. There was a continuous increase observed in the quantity of the $H_2$ consumed during reduction for L5RhZ (see Fig. 14b) as for L2RhZ (Fig. 14a). This increase in the $H_2$ consumption is partly due to the increase in the reduction of the lanthanum zirconate at 500 °C and partly due to the reduction of Rh metal that interacted less strongly with the pyrochlore structure.

The temperature of reduction of spent LZ did not change significantly as compared to the reduction of the fresh LZ. The TPR profiles of the fresh catalyst and the spent catalysts are not shown here due to the similarity between them and lack of any additional insight.

The $H_2$ consumption for the reduction of the spent catalyst is in direct proportion to the temperature at which the DRM reforming reaction was conducted. Because the DRM reaction conditions are extremely reducing, this may have caused some of the Rh to destabilize from the bulk of the crystal and diffuse to the surface of the catalyst. As the Rh loading increased, the maximum capacity of the pyrochlore structure for Rh at the B site was exceeded, causing Rh atoms to break the coordination with the neighboring La, Zr, Rh, and O atoms in the bulk and move to the surface and form weakly bonded Rh, with a reducibility comparable to supported Rh catalysts.

*XRD of the spent catalysts from DRM followed by TPO and TPR*

After conducting TPR on the spent L5RhZ pyrochlore, the changes in their crystalline structure were studied by conducting XRD over these catalysts. We are not aware of any paper in the literature discussing these series of experiments over pyrochlores for DRM. The diffraction pattern

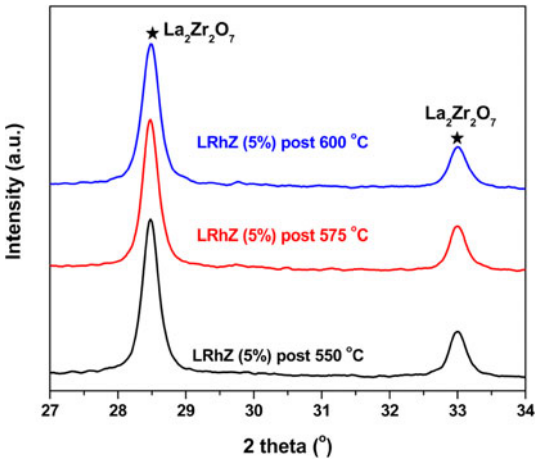


**Fig. 15** Plot of the XRD pattern for the L5RhZ pyrochlores spent for DRM at 500, 575, and 600 °C with GHSV = 48,000 mL/$g_{cat}$/h at 1 atm followed by TPO and TPR up to 950 °C showing in particular that the $LaRhO_3$ perovskite peak vanishes after TPR

of these reduced L5RhZ pyrochlores did not show the presence of perovskite ($LaRhO_3$) phase (in Fig. 15). The observable perovskite phase ($LaRhO_3$) that was formed in the L5RhZ pyrochlore after the TPO of the spent catalysts, appears to be reduced by TPR to amorphous form which could not be detected by the X-rays during diffraction.

## Conclusion

The XRD studies of the freshly calcined pyrochlores show a peak for $LaRhO_3$ which was observed for L5RhZ pyrochlore, possibly due to the higher Rh loading which led to separation of the excess Rh into the perovskite phase. XPS shows that rhodium is present primarily as $Rh^{+3}$ species on the surface of L2RhZ and L5RhZ and that there was no major local surface aggregation due to higher concentration of Rh on the surface of L5RhZ. TPR results of the fresh catalysts show that the total reducibility of the pyrochlores (mg $H_2$ consumed/$g_{cat}$) increased with increasing Rh substitution. The conversion of $CH_4$ and $CO_2$ and the resultant product $H_2$/CO ratio over a series of substituted lanthanum zirconate pyrochlores increased with Rh loading and reaction temperature. The TPO of the catalysts after DRM shows that carbon formation decreases with an increase in Rh loading and increasing reaction temperature. The post reaction XRD plots show that there was no apparent change observed in the LZ and L2RhZ structures. However, for spent L5RhZ, the higher Rh loading could have caused the excess metal to separate out as a perovskite phase. When these spent L5RhZ pyrochlores were subjected to TPR after the TPO, the reduction temperature of the Rh was lower than that of the freshly calcined catalysts and there was also an observable increase in the $H_2$ consumption. This was attributed to the diffusion of Rh metal from the bulk of the structure to the surface. However, the XRD pattern of the reduced spent L5RhZ pyrochlore did not show a perovskite phase, likely because the $LaRhO_3$ phase was reduced to some non-crystalline form. This result is novel and gives an insight into the behavior of Rh in the pyrochlore structure under alternating reducing (DRM and TPR) and oxidizing conditions. To our knowledge, this disappearance of perovskite ($LaRhO_3$) phase by alternative oxidation and reduction treatment has not been reported in the literature particularly for pyrochlores catalyzing DRM.

**Acknowledgments** This material is based upon work supported as part of the Center for Atomic Level Catalyst Design, an Energy Frontier Research Center funded by the U.S. Department of Energy, Office of Science, Office of Basic Energy Sciences under Award Number DE-SC0001058. We thank Ms. Kim Hutchison at North Carolina State University, Ms. Wanda LeBlanc at Louisiana State University and Dr. Nachal Subramanian at Georgia Tech (currently) for helping in getting the ICP, XRD, and XPS data, respectively.



## References

1. Subramanian MA, Aravamudan G, Rao GVS (1983) Oxide pyrochlores—a review. Prog Solid State Chem 15(2):55–143. doi:10.1016/0079-6786(83)90001-8
2. Wilde PJ, Catlow CRA (1998) Defects and diffusion in pyrochlore structured oxides. Solid State Ionics 112(3–4):173–183. doi:10.1016/s0167-2738(98)00190-8
3. Whittle KR, Cranswick LMD, Redfern SAT, Swainson IP, Lumpkin GR (2009) Lanthanum pyrochlores and the effect of yttrium addition in the systems La(2-x)Y(x)Zr(2)O(7) and La(2-x)Y(x)Hf(2)O(7). J Solid State Chem 182(3):442–450. doi:10.1016/j.jssc.2008.11.008
4. Schmalle HW, Williams T, Reller A, Linden A, Bednorz JG (1993) The twin structure of $La_2Ti_2O_7$—X-ray and transmission electron-microscopy studies. Acta Crystallogr Sect B Struct Commun 49:235–244. doi:10.1107/s010876819200987x
5. Pakhare D, Haynes D, Shekhawat D, Spivey J (2012) Role of metal substitution in lanthanum zirconate pyrochlores ($La_2Zr_2O_7$) for dry ($CO_2$) reforming of methane (DRM). Appl Petrochem Res 2(1–2):27–35. doi:10.1007/s13203-012-0014-6
6. Iyer MV, Norcio LP, Kugler EL, Dadyburjor DB (2003) Kinetic modeling for methane reforming with carbon dioxide over a mixed-metal carbide catalyst. Ind Eng Chem Res 42(12):2712–2721. doi:10.1021/ie020677q
7. Kumar N, Smith ML, Spivey JJ (2012) Characterization and testing of silica-supported cobalt-palladium catalysts for conversion of syngas to oxygenates. J Catal 289:218–226. doi:10.1016/j.jcat.2012.02.011
8. Bradford MCJ, Vannice MA (1996) Catalytic reforming of methane with carbon dioxide over nickel catalysts II. Reaction Appl Catal A 142(1):97–122. doi:10.1016/0926-860x(96)00066-x

9. Brungs AJ, York APE, Claridge JB, Marquez-Alvarez C, Green MLH (2000) Dry reforming of methane to synthesis gas over supported molybdenum carbide catalysts. Catal Lett 70(3–4): 117–122. doi:10.1023/a:1018829116093
10. Coronel L, Munera JF, Lombardo EA, Cornaglia LM (2011) Pd based membrane reactor for ultra pure hydrogen production through the dry reforming of methane. Experimental and modeling studies. Appl Catal A 400(1–2):185–194. doi:10.1016/j.apcata.2011.04.030
11. de Arauj GC, de Lima SM, Assaf JM, Pena MA, Garcia Fierro JL, MdC Rangel (2008) Catalytic evaluation of perovskite-type oxide $LaNi_1$-x$RuxO_3$ in methane dry reforming. Catal Today 133:129–135. doi:10.1016/j.cattod.2007.12.049
12. Bradford MCJ, Vannice MA (1999) $CO_2$ reforming of $CH_4$. Catal Rev Sci Eng 41(1):1–42. doi:10.1081/cr-100101948
13. Subramanian ND, Gao J, Mo XH, Goodwin JG, Torres W, Spivey JJ (2010) La and/or V oxide promoted Rh/SiO2 catalysts: effect of temperature, H-2/CO ratio, space velocity, and pressure on ethanol selectivity from syngas. J Catal 272(2):204–209. doi:10.1016/j.jcat.2010.03.019
14. Schuurman Y, Mirodatos C, Ferreira-Aparicio P, Rodriguez-Ramos I, Guerrero-Ruiz A (2000) Bifunctional pathways in the carbon dioxide reforming of methane over MgO-promoted Ru/C catalysts. Catal Lett 66(1–2):33–37. doi:10.1023/a:1019022917507
15. Ross JRH (2005) Natural gas reforming and $CO_2$ mitigation. Catal Today 100(1–2):151–158. doi:10.1016/j.cattod.2005.03.044
16. Gadalla AM, Bower B (1988) The role of catalyst support on the activity of nickel for reforming methane with $CO_2$. Chem Eng Sci 43(11):3049–3062. doi:10.1016/0009-2509(88)80058-7
17. Gallego GS, Batiot-Dupeyrat C, Barrault J, Florez E, Mondragon F (2008) Dry reforming of methane over LaNi1-yByO3 ± delta(B = Mg, Co) perovskites used as catalyst precursor. Appl Catal A 334(1–2):251–258. doi:10.1016/j.apcata.2007.10.010
18. Hou ZY, Zheng XM, Yashima T (2005) High coke-resistance of K-Ca-promoted Ni/alpha-$Al_2O_3$ catalyst for $CH_4$ reforming with $CO_2$. React Kinet Catal Lett 84(2):229–235
19. Haynes DJ, Berry DA, Shekhawat D, Spivey JJ (2008) Catalytic partial oxidation of *n*-tetradecane using pyrochlores: effect of Rh and Sr substitution. Catal Today 136(3–4):206–213. doi:10.1016/j.cattod.2008.02.012
20. Diaz-Guillen JA, Diaz-Guillen AR, Padmasree KP, Almanza JM, Fuentes AF, Santamaria J, Leon C (2008) Synthesis and electrical properties of the pyrochlore-type Gd(2-y)La(y)Zr(2)O(7) solid solution. Bol Soc Esp Ceram Vidr 47(3):159–164
21. Ashcroft AT, Cheetham AK, Jones RH, Natarajan S, Thomas JM, Waller D, Clark SM (1993) An insitu, energy-dispersive X-ray-diffraction study of natural-gas conversion by $CO_2$ reforming. J Phys Chem 97(13):3355–3358. doi:10.1021/j100115a044
22. Haynes DJ, Campos A, Berry DA, Shekhawat D, Roy A, Spivey JJ (2010) Catalytic partial oxidation of a diesel surrogate fuel using an Ru-substituted pyrochlore. Catal Today 155(1–2):84–91. doi:10.1016/j.cattod.2009.03.025
23. Hayakawa I, Kamizono H (1993) Durability of an $La_2Zr_2O_7$ waste form containing various amounts of simulated HLW elements. J Nucl Mater 202(1–2):163–168. doi:10.1016/0022-3115(93)90039-2
24. Sheng PY, Chiu WW, Yee A, Morrison SJ, Idriss H (2007) Hydrogen production from ethanol over bimetallic Rh-M/$CeO_2$ (M = Pd or Pt). Catal Today 129(3–4):313–321. doi:10.1016/j.cattod.2006.09.040
25. Eriksson S, Rojas S, Boutonnet M, Fierro JLG (2007) Effect of Ce-doping on Rh/$ZrO_2$ catalysts for partial oxidation of methane. Appl Catal A 326(1):8–16. doi:10.1016/j.apcata.2007.03.019
26. Larichev YV, Netskina OV, Komova OV, Simagina VI (2010) Comparative XPS study of Rh/Al(2)O(3) and Rh/TiO(2) as catalysts for NaBH(4) hydrolysis. Int J Hydrogen Energy 35(13):6501–6507. doi:10.1016/j.ijhydene.2010.04.048
27. Wang Y, Song Z, Ma D, Luo HY, Liang DB, Bao XH (1999) Characterization of Rh-based catalysts with EPR, TPR, IR and XPS. J Mol Catal A Chem 149(1–2):51–61. doi:10.1016/s1381-1169(99)00181-8
28. Sandell A, Libuda J, Bruhwiler PA, Andersson S, Maxwell AJ, Baumer M, Martensson N, Freund HJ (1996) Interaction of CO with Pd clusters supported on a thin alumina film. J Vac Sci Technol A Vac Surf Films 14(3):1546–1551. doi:10.1116/1.580293
29. Stoychev D, Valov I, Stefanov P, Atanasova G, Stoycheva M, Marinova T (2003) Electrochemical growth of thin $La_2O_3$ films on oxide and metal surfaces. Mater Sci Eng C Biomimetic Supramol Syst 23(1–2):123–128. doi:10.1016/s0928-4931(02)00261-8
30. Wang HR, Chen YQ, Zhang QL, Zhu QC, Gong MC, Zhao M (2009) Catalytic methanol decomposition to carbon monoxide and hydrogen over Pd/CeO(2)-ZrO(2)-La(2)O(3) with different Ce/Zr molar ratios. J Nat Gas Chem 18(2):211–216. doi:10.1016/s1003-9953(08)60109-7
31. Hoang DL, Lieske H (2000) Temperature-programmed reduction study of chromium oxide supported on zirconia and lanthana-zirconia. Thermochim Acta 345(1):93–99. doi:10.1016/s0040-6031(99)00385-8
32. Wei JM, Iglesia E (2004) Isotopic and kinetic assessment of the mechanism of reactions of $CH_4$ with $CO_2$ or $H_2O$ to form synthesis gas and carbon on nickel catalysts. J Catal 224(2):370–383. doi:10.1016/j.jcat.2004.02.032
33. Bitter JH, Seshan K, Lercher JA (2000) On the contribution of X-ray absorption spectroscopy to explore structure and activity relations of Pt/$ZrO_2$ catalysts for $CO_2$/$CH_4$ reforming. Top Catal 10(3–4):295–305. doi:10.1023/a:1019149025242
34. Wei JM, Iglesia E (2004) Structural requirements and reaction pathways in methane activation and chemical conversion catalyzed by rhodium. J Catal 225(1):116–127. doi:10.1016/j.jcat.2003.09.030
35. Zhang ZL, Verykios XE (1996) Mechanistic aspects of carbon dioxide reforming of methane to synthesis gas over Ni catalysts. Catal Lett 38(3–4):175–179. doi:10.1007/bf00806565
36. Fan M-S, Abdullah AZ, Bhatia S (2009) Catalytic technology for carbon dioxide reforming of methane to synthesis gas. ChemCatChem 1(2):192–208. doi:10.1002/cctc.200900025
37. Nakamura J, Aikawa K, Sato K, Uchijima T (1994) Role of support in reforming of $CH_4$ with $CO_2$ over Rh catalysts. Catal Lett 25(3–4):265–270. doi:10.1007/bf00816306
38. Zhang ZL, Tsipouriari VA, Efstathiou AM, Verykios XE (1996) Reforming of methane with carbon dioxide to synthesis gas over supported rhodium catalysts I. Effects of support and metal crystallite size on reaction activity and deactivation characteristics. J Catal 158(1):51–63. doi:10.1006/jcat.1996.0005
39. Shamsi A, Baltrus JR, Spivey JJ (2005) Characterization of coke deposited on Pt/alumina catalyst during reforming of liquid hydrocarbons. Appl Catal A 293:145–152. doi:10.1016/j.apcata.2005.07.002
40. Barbier J (1986) Deactivation of reforming catalysts by coking—a review. Appl Catal 23(2):225–243. doi:10.1016/s0166-9834(00)81294-4
41. Sarusi I, Fodor K, Baan K, Oszko A, Potari G, Erdohelyi A (2011) CO(2) reforming of CH(4) on doped Rh/Al(2)O(3) catalysts. Catal Today 171(1):132–139. doi:10.1016/j.cattod.2011.03.075